



Kinetics of HSA crystallization and its relationship with the phase diagram

Cara Buchholz, Lara F. Reichart, Furio Surfaro, Ralph Maier, Fajun Zhang, Alexander Gerlach, Frank Schreiber*

Institut für Angewandte Physik, Universität Tübingen, Auf der Morgenstelle 10, Tübingen 72076, Germany

ARTICLE INFO

Communicated by P.G. Vekilov

Keywords:

B1. Proteins
A1. Crystallization
A1. Optical microscopy
A1. Kinetics
A1. Phase diagram
B1. Multivalent ions

ABSTRACT

Using the protein human serum albumin (HSA) and the trivalent salt cerium chloride (CeCl_3) to tune the effective interactions, we induce crystallization and connect the crystallization kinetics to different regions of the phase diagram. The nucleation density, the nucleation rate, as well as the crystal size show maxima slightly above the specific salt concentration c^* for aggregation. The comparison with data of the reduced second virial coefficient suggests that B_2/B_2^{HS} alone is insufficient to explain the observed trends. We thus discuss further aspects impacting the crystallization behavior. We are able to link and distinguish the kinetic regimes regarding their relative distance to phase boundaries, namely c^* as well as the liquid–liquid phase separation (LLPS) border.

1. Introduction

A major challenge in understanding the structure of proteins, and thus their function, is acquiring high quality crystals suitable for diffraction [1]. This is of key importance in various areas ranging from pharmacy and medicine to structural biology. Yet, crystallization remains difficult to predict and control due to the complex interactions that proteins exhibit in solution and the associated non-trivial phase behavior [2–5]. A particular challenge for the fundamental understanding is the relationship of the phase diagram with the crystallization kinetics and resulting density and size of crystals [5–15].

Human serum albumin (HSA) is the most abundant protein in the human blood stream and has many important physiological functions, from maintaining the osmotic pressure to carrying small molecules [16, 17]. Since HSA is a globular and net-negatively charged protein at neutral pH, it is an ideal object to study cation-induced crystallization. Specifically multivalent ions offer an intriguing way of inducing crystallization, as they can trigger effective attractive interactions, the strength of which can be controlled by the salt concentration c_s [18–23].

Trivalent ions can give rise to reentrant condensation (RC) phase behavior of the protein solutions [20]. At neutral pH, the proteins exhibit a net repulsive force due to their charge and the aqueous solution is clear (regime I). For c_s above the first specific salt concentration (c^*), the ions bind to the proteins, diminishing their net charge, and may even facilitate the bridging of proteins, causing the proteins to aggregate and the solution to become turbid. This second regime (regime II) can also consist of different condensed phases, namely a

dense and a dilute protein solution caused by a metastable liquid–liquid phase separation (LLPS) [20]. As c_s is further increased above a second specific concentration (c^{**}), more ions bind to the protein, causing the proteins to undergo an effective charge inversion (regime III) and the solution to be clear again [18,24].

Previous work on the HSA- CeCl_3 system focused on the crystallization pathway and the role of LLPS [25]. Nucleation mostly occurs in regime II of the phase diagram, near the LLPS loop [26]. Apparently, the dense liquid phase (DLP) acts as a reservoir for nucleation [25].

In the present paper, we shed light on the crystallization process by studying the kinetics. In fact, connecting the kinetics to the phase behavior is a key ingredient for the overall understanding of the crystallization and the fine-tuning of, e.g., nucleation probability, crystal size and quality.

This paper is organized as follows. In Section 2, the materials and the experimental methods are explained. Section 3 is dedicated to the results, where we first explain in detail the phase diagram with its peculiarities and then the kinetic behavior in different regions of the phase diagram. The conclusions are presented in Section 4. A number of complementary plots of the large body of data is provided in the Supplementary Information.

2. Materials and experimental methods

2.1. Materials

HSA and CeCl_3 were purchased from Sigma-Aldrich, now Merck, with guaranteed purities of 97% for HSA (product no. A9511) and

* Corresponding author.

E-mail address: frank.schreiber@uni-tuebingen.de (F. Schreiber).

99.99% for CeCl_3 (product no. 429406). Protein and salt were used as received without further purification. The stock solutions were prepared by dissolving weighed amounts of protein or salt powder in deionized (18.2 M Ω) and degassed Millipore water, respectively, at room temperature. A freshly prepared protein solution was incubated overnight to ensure the complete dissolution of the protein powder. Subsequently, the protein concentration was determined by UV-Vis-spectroscopy, using an extinction coefficient of HSA of $\epsilon = 0.531 \text{ ml mg}^{-1} \text{ cm}^{-1}$ at a wavelength of $\lambda = 278 \text{ nm}$ [27]. The HSA stock solutions were kept in the fridge for up to three weeks. The CeCl_3 solution was stored at room temperature and was used for all experiments in this study.

We note that for protein work, generally there is a certain batch-to-batch variation. The results presented here are consistent within one batch, and general statements apply to other batches as well.

2.2. Methods

2.2.1. Determination of phase boundaries and crystallization conditions

Since in regime II the effective intermolecular interactions are mostly attractive and crystallization is facilitated by the multivalent cations, crystallization is expected to occur predominantly here. Thus, conditions within regime II were chosen for the crystallization experiments. To ensure that the chosen salt concentrations are located within the second regime, the phase boundaries of the second regime (c^* and c^{**}) were determined by visual inspection of a dilution series (similar to Ref. [25]). For all experiments, the temperature was kept constant at $23 \pm 0.5^\circ\text{C}$.

2.2.2. Optical microscopy

For optical microscopy experiments, fresh sample solutions were prepared. After adding the salt solution, the required amount of volume was transferred into spacers, which were previously mounted on a glass slide and subsequently covered with a cover slide. These spacers composed of double-sided adhesive film were purchased from Thermo Scientific™ with an area of 1 cm^2 , a height of 0.25 mm and $25 \mu\text{l}$ volume.

The samples were investigated using a bright-field optical microscope (Axio Scope.A1, Carl Zeiss AG). Images were recorded by a microscope-included camera (AxioCam ICc5, Carl Zeiss AG) in combination with the software ZEISS ZEN 3.2. The same software was also used for length and area measurements of the crystals. The diameter of a crystal could be determined with an error of $\pm 5 \mu\text{m}$.

Crystallization was observed at fixed time intervals from a few hours after preparation to a maximum of 14 days. At these times, images were recorded, and the number of crystals grown inside the spacer was counted. For the crystal counting, a 10x objective was used, which translates into the smallest detectable crystal size of about $25 \mu\text{m}$. The crystal counting comes with a certain inherent error, because the nuclei only become visible with a certain time delay, which has to be considered when discussing the temporal onset of nucleation. Nevertheless, the nucleation rate can be obtained by counting the visible crystals under the assumption that every critical nucleus grows at the same rate into a crystal of detectable size [28,29].

To acquire three-dimensional (3D) complementary images of the crystals, images of selected samples were taken with a confocal fluorescence microscope (Leica SP8). For this, the samples had to be inverted, since the microscope was mounted on an inverted microscope body. HSA shows an intrinsic fluorescence, which originates from the tryptophan (Trp) 214 residue of the protein [30]. The excitation laser employed had a wavelength of 488 nm , and a 10x objective (air) was used. Three-dimensional images were generated from an acquired z-stack of confocal images. For this purpose, the software Fiji (version ImageJ 1.53c) [31] and the plugins *Volume Viewer* and *3D Viewer* [32] were used. Contrast and brightness were adjusted in Fiji [31].

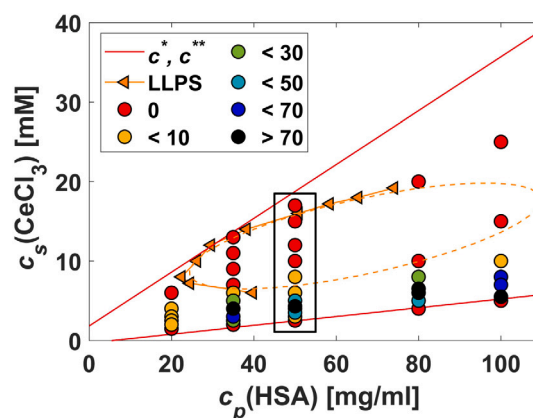


Fig. 1. Phase diagram with the phase boundaries c^* and c^{**} . The number of crystals per cm^2 (i.e., the nucleation density) after 14 days is represented by differently colored filled circles. The nucleation density for the respective conditions within the HSA/ CeCl_3 phase diagram is indicated according to the legend. Samples at $c_p = 20, 35, 50, 80$ and 100 mg/ml with varying c_s were investigated in spacers with a volume of $25 \mu\text{l}$. The error of the counted crystal numbers is estimated to be about 10%. The vertical box around $c_p = 50 \text{ mg/ml}$ indicates the conditions employed in Fig. 2. (For interpretation of the references to color in this figure legend, the reader is referred to the web version of this article.)

3. Results and discussion

To establish a connection between the crystallization kinetics and the phase diagram, the crystallization conditions were determined by systematically varying the protein and salt concentration. Fig. 1 can be regarded as a multidimensional map of the HSA- CeCl_3 crystallization regime that is used as a guide for the subsequent kinetic analysis (Section 3.2). The studied observables along a fixed protein concentration of $c_p = 50 \text{ mg/ml}$, namely nucleation density, kinetic growth rate k , and maximum crystal size are compiled in Fig. 2.

3.1. Phase diagram and crystallization conditions

Fig. 1 shows the experimental phase diagram with the phase boundaries c^* and c^{**} and the number of crystals (14 days after preparation in spacers with $25 \mu\text{l}$ volume) found at different conditions across the phase diagram.

This already leads to several important qualitative observations. First of all, crystallization was observed only in the lower part of the second regime. In general, this is in good agreement with previous experimental results that crystallization is only observed in regime II. Here, the value of the reduced second virial coefficient B_2/B_2^{HS} of the bulk solution is clearly negative, indicating a net attraction between proteins (see Ref. [26]). The model of ion-activated attractive patches can successfully describe the underlying mechanism of attraction and phase behavior [24]. The absence of HSA crystallization at high c_s may be caused by the high occupation of binding sites by metal ions, which could block the protein-protein contacts or change the crystallization pathway [18,19,26].

Second, with increasing c_p , a broadening of the second regime can be observed. However, the conditions at which crystals were found do not reach significantly higher c_s values with increasing c_p (Fig. 1). This means that the width of the second regime in terms of absolute salt concentration is not reflected in a broader c_s -window for crystallization. Reasons for this observation might be the strong aggregation of proteins, which is observed at high c_p . This might drive proteins to aggregate too quickly, leading to unfavorable binding and blocking of surface sites of more productive crystal growth [33]. In addition, the aggregates formed might be rather stable, which would drastically lower the supersaturation of the remaining solution and inhibit crystal nucleation.

Last, as can be seen from Figs. 1 and 2b, the nucleation density exhibits a sharp maximum shortly above c^* and then decays rapidly upon increasing c_s . Data of the crystal number density for a fixed c_p of 50 mg/ml is given in Fig. 2b. In this region, the value of the reduced second virial coefficient B_2/B_2^{HS} of the bulk solution corresponds to strong attractive interactions (Ref. [26]); however, the pronounced nucleation density maximum from Fig. 2b is not reflected in a sharp minimum of the B_2/B_2^{HS} values. Instead, the minimum extends to far higher c_s . This suggests that the values of the second virial coefficient indeed indicate the window of conditions suitable for crystallization for our system as phenomenologically predicted by George and Wilson [34], but are not sufficient to predict the details of nucleation densities and the corresponding kinetics of our system. The steep increase in nucleation density crossing c^* is indeed reflected in a sharp decrease in the B_2/B_2^{HS} values, however, the nucleation density shows a much more dramatic decrease after reaching maximum values than B_2/B_2^{HS} [26]. In particular, for directional bonds and localized attractive sites as in our system (see also Ref. [24]), it is clear that there will be subtleties (anisotropic interactions) that will not be captured in B_2/B_2^{HS} . We also note that it is expected that for a given crystal structure, a certain stoichiometry will be optimal [18,24,25]. Therefore, even if there are still attractive interactions when moving above a certain salt concentration, the stoichiometry might no longer be ideal for supporting the growth of the crystal.

3.2. Nucleation kinetics

The detailed characterization of the crystallization regime of the HSA-CeCl₃ of the previous section permits a kinetic study of the crystal nucleation and growth. Here we investigate the effect of the protein and salt concentration on the kinetic parameters (Sections 3.2.2 and 3.2.3), as well as on size and shape of the crystals (Section 3.3).

3.2.1. Shape of the kinetic curve

Fig. 3 shows nucleation densities as a function of time for different conditions at $c_p = 50$ mg/ml. We find that the number of crystals increases exponentially after an initial lag time corresponding to t_c and then saturates (see also Figure A.7 in the SI for other c_p). To extract quantitative kinetic parameters, such as the characteristic growth rate k and the incubation parameter t_c , the data are fitted with a sigmoid function [35]:

$$n(t) = \frac{n_s}{(1 + \exp(-k \cdot (t - t_c)))} \quad (1)$$

where n_s is the saturated nuclei number density. We note that for very small n_s , a fit with the sigmoidal curve is only reasonable in limits due to the high relative error in the quantification of the crystal numbers. Still, for all conditions across the phase diagram, the sigmoidal function can be considered a good fit. The fit qualities R^2 of the curves in Fig. 3 and A.7 lie between 0.9138 and 0.9971.

From the fitted curves, the incubation parameter t_c , as well as the characteristic nucleation rate k could be obtained. The time t_c is marked with a red star for each curve in Fig. 3. The following sections investigate how the kinetic rate k is controlled by the protein concentration and the salt concentration.

3.2.2. Kinetic analysis

In order to rationalize the kinetic parameters and put them into a context, we will now discuss a model for their dependence on c_p and c_s . We emphasize that this scaling (inspired by the dynamics study in Ref. [36]) is certainly oversimplified, but serves to organize the data. Both the protein and the relative salt concentration are expected to affect the kinetics of the HSA-CeCl₃ crystallization. Regarding the effect of c_p , we expect that the number of proteins in solution is proportional to the flux, *i.e.*, the number of molecules that reach a surface in a given time. In the present system, proteins from the bulk solution reach the nuclei's surface and are incorporated into the crystal lattice. For the

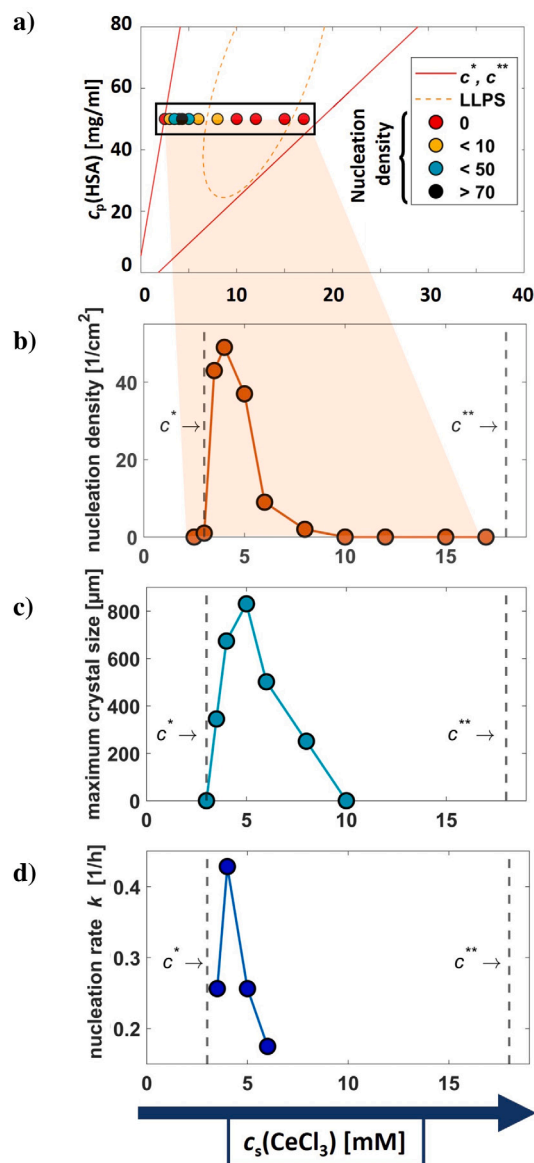


Fig. 2. Phase diagram and observables of the crystallization process as a function of c_s . (a) Section of the phase diagram (rotated by 90° relative to Fig. 1), highlighting the conditions at $c_p = 50$ mg/ml (horizontal box), (b) nucleation density after 14 days, (c) maximum crystal size after 14 days and (d) nucleation rate k .

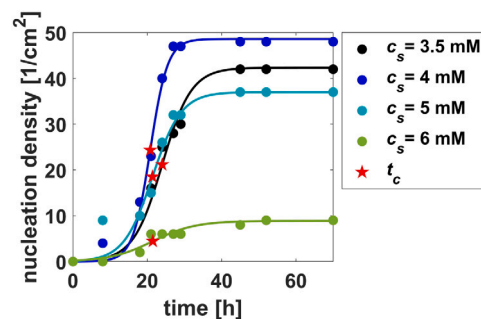


Fig. 3. Nucleation density (number of crystals per cm²) as a function of time for four different salt concentrations at $c_p = 50$ mg/ml. The curves are fitted with a sigmoid function (see Eq. (1)). Their inflection point represents t_c , the incubation parameter (marked as a red star). The error of the counted crystal numbers is estimated to be about 10%.

sake of the next step in the analysis, we assume that the higher the flux, the faster are the nucleation kinetics. This can be applied to both, a fast onset of the nucleation (small t_c) and a high nucleation rate (high k). With this, we obtain the relation

$$c_p \propto 1/t_c \propto k. \quad (2)$$

The scalability of both, t_c and k with the protein concentration can be tested in the kinetic analysis. This means that for otherwise comparable conditions, calculated values of k/c_p and likewise $t_c \cdot c_p$ should be constant within this simple picture.

The term “comparable conditions” here refers to a consistent driving force, which is mostly controlled by c_s in this system, as it dominantly determines the strength of the effective interactions. Within the framework of our simplified analysis, the following considerations are made. In the present system, with its rich phase behavior, we expect strong differences in the interactions at different locations in the phase diagram [37,38]. We can speculate that the distance to the phase boundaries is an important measure, as it can impact the nucleation mechanism and its kinetics [37,38]. In the spirit of Soraruf et al. [36], we can employ the ratio between salt and protein concentration (c_s/c_p) for comparing different samples, since this corresponds to approximately constant distances to the phase transition boundaries of c^* and the LLPS region and with that comparable driving forces, at least within a certain window of conditions.

Eq. (2) is supported by Barlow et al. as they assumed the characteristic rate k to be proportional to the initial protein concentration: $k = \text{const} \cdot c_p$ [39]. Furthermore, Schmit et al. developed a theory that predicts the nucleation rates (as well as crystal growth speed) to increase with the protein concentration [33]. This will be tested in the following.

3.2.3. Dependence of kinetics on the protein concentration

For the study of the kinetic dependence on protein concentration, the c_s/c_p ratio, as a measure of the position in the phase diagram and with that a measure of the effective interactions, is kept constant. For all c_s/c_p , most values of k/c_p lie between 0.002 and 0.008 $\text{ml mg}^{-1} \text{h}^{-1}$. As an example, Fig. 4a displays the values of k/c_p as a function of c_p for $c_s/c_p = 6.8$ (see Figures A.8 and A.9 for the corresponding plots at other c_s/c_p values). Fig. 4b illustrates the corresponding conditions in the phase diagram of the present system. Taking the error bars into account, it can be further observed that most data points show indeed little variation in the c_p range investigated, which is consistent with the model assumptions.

It has to be noted that at all c_s/c_p (apart from $c_s/c_p = 5.8$), there are deviations from $k/c_p = \text{const}$ at high protein concentrations (see Fig. 4, A.8 and A.9), i.e., indeed the range of the validity of the model is limited, as expected. In essence, at $c_p \geq 65 \text{ mg/ml}$, the values of k/c_p are significantly smaller than at lower c_p . This deviation might be caused by the fast aggregation at high c_p , which can lead to non-productive binding of protein molecules and hence might impact the nucleation process [33]. Another conceivable reason would be that the (amorphous) aggregates are too large at high c_p and take longer to solubilize again (or some might even be insoluble), which would lower the supersaturation of the solution and thus could slow down the nucleation rate. Galkin and Vekilov reported similar deviations in the nucleation rates at high protein concentrations (high supersaturations) for lysozyme [40,41].

Nonetheless, we find that the values of k/c_p are roughly in the same range, confirming the assumption that k is proportional to the initial c_p for similar positions in the phase diagram (constant c_s/c_p), corresponding to comparable strengths of salt-induced attractive forces. This suggests that a similar mechanism underlies the nucleation process under these conditions and its kinetic rate k is limited by the flux of molecules to the surface of nuclei (which is proportional to c_p), meaning the more material is in solution, the higher the characteristic rate of the nucleation process. Thus, nucleation and crystal growth

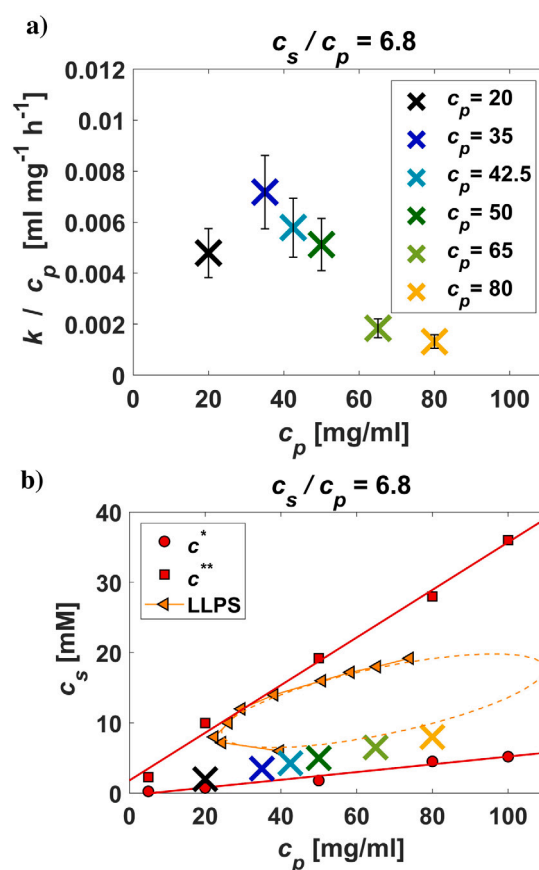


Fig. 4. Connection of crystallization kinetics with the phase diagram: (a) k/c_p as a function of c_p for samples with a constant $c_s/c_p = 6.8$. (b) Corresponding locations in the phase diagram. Note that the data points are chosen with constant c_s/c_p with increasing c_p . The error of k is estimated to be about 20% (but might be larger for individual conditions) and is indicated by the error bars.

seem to be diffusion limited. Hence, the protein molecules are expected to orient themselves quickly and attach to the crystal lattice in a proper orientation faster than the diffusion towards the crystal surface takes place. Similar observations were already made for protein and small molecule crystals [42]. In contrast, for lysozyme, the kinetic incorporation of proteins was reported to be the rate-limiting step [43].

3.2.4. Dependence of kinetics on the salt concentration

To study the influence of the salt concentration on the nucleation kinetics, we analyze the nucleation rate at a constant protein concentration (see Fig. 2d) of $c_p = 50 \text{ mg/ml}$. As c_s is increased, two phase transitions, the c^* border and the LLPS are found in the phase diagram not far away from each other in the present system (see Fig. 1).

It was demonstrated for various systems that close to (or inside) the LLPS regime, the kinetics of the crystallization speed up [4,37,44,45]. This may have several reasons. First, simulations, theoretical studies and experiments showed an enhanced crystallization behavior close to the critical point due to density fluctuations [4,37,46]. Second, the interfacial energy between dense phase and crystal can be lower than between initial solution and crystal, resulting in a decreased activation energy barrier for the crystallization process [7]. Last, the surface of the dense droplets can act as heterogeneous nucleation site [47].

For the present system, unfortunately only an approximate LLPS boundary is available for the conditions $c_p = 50 \text{ mg/ml}$ (see extrapolated LLPS loop in Fig. 1). A macroscopic observation (in the bulk) of the phase separation, such as the one performed for a similar system (bovine serum albumin with CeCl_3 , Ref. [48]) was not possible,

because the amount of dense phase was either too small for detection or the liquid dense phase was accompanied by aggregates. Alternatively, we employed a microscopic investigation of LLPS at certain salt concentrations at $c_p = 50$ mg/ml. From light microscopy images, it becomes apparent that phase separation occurs over a broad c_s range at $c_p = 50$ mg/ml. Note that due to possible confinement effects of the spacers, the phase boundaries might be shifted slightly compared to the bulk. Phase separation on the microscopy slides is observed in the form of dense droplets at almost all salt concentrations in the second regime, *i.e.*, even at lower and higher c_s values than crystallization is observed.

Interestingly, variations in the amount of droplets (phase separation) are noticeable when c_s is varied. In the c_s -range where the kinetic parameters and the nucleation density decrease, we see an increase in the amount of microscopic dense phase droplets. One possible explanation for this is given by the fact that the nucleation process and the resulting crystallization is observed to appear in the dilute phase [25]. Consequently, where a new metastable dense phase is formed, the resulting concentration in the dilute phase is lower. Thus, if the rate of crystallization is dependent on the number of proteins in the dilute phase, the formation of a dense phase leads to slower kinetics of the crystallization channel due to the existence of a competing kinetic channel, *i.e.* the conversion to the dense phase [4].

There is some analogy with the simulations performed by Lutsko of macromolecules in solution, which are in agreement with the slower nucleation rates [49]. He observed a dense-solution (liquid-like) layer forming on the surface of the crystal so that the energy barrier is associated with the freezing transition and multiple barriers must be overcome leading to slower nucleation rates. Concerning a potential effect of the LLPS on the nucleation and growth of the crystals, it remains unclear whether the existence of LLPS has an influence or possible effects compete, since we find microscopic LLPS for all crystallizing conditions in the present system.

Apart from the decrease in protein concentration within the dilute phase compared to the initial solution due to LLPS, a possible explanation could be the higher occupation of protein binding sites (by Ce^{3+} ions) and associated changes in the interactions with increasing c_s , which potentially causes the slowing down of the characteristic rate.

In addition to the occurrence of LLPS and possible related effects on the crystallization behavior, the salt concentration is key in the process. Importantly, the multivalent ions are not only a way to control the interactions, but they are also incorporated into the crystal [25], for which it is likely that certain ratios/stoichiometries are preferred. With these two mechanisms at play (interactions and stoichiometry), it appears rather likely that crystallization (apart from being a nonlinear process that obviously does not exactly have to follow B_2/B_2^{HS}) depends very sensitively on c_s , and that there may be a rather narrow “sweet spot” of nucleation.

It has to be noted here that we find the systematic behavior for each given batch of protein. The absolute nucleation rate appears to be highly sensitive to impurities in the protein solution (see comment in Section 2.1). Nevertheless, the observation that the kinetic rate exhibits a sharp maximum above c^* upon increasing c_s is a robust finding, reflecting the clear salt-specific trend already observed in nucleation density.

3.2.5. Evolution of size and shape

Having explained where in our phase diagram crystals are able to nucleate, we have a closer look at the size and the shape of the individual crystals. Interestingly, in contrast to other systems we have studied, only one type of morphology was observed for the present system [18,19,48,50,51]. The crystals of HSA crystallized in the presence of $CeCl_3$ show a lentil-like morphology for all c_p and c_s as revealed by light and fluorescence microscopy (Fig. 5).

In addition to observing ensemble-averaged kinetics, also the growth of individual crystals was tracked over time. Typical growth curves of individual crystals are depicted in Figure A.12. Since the

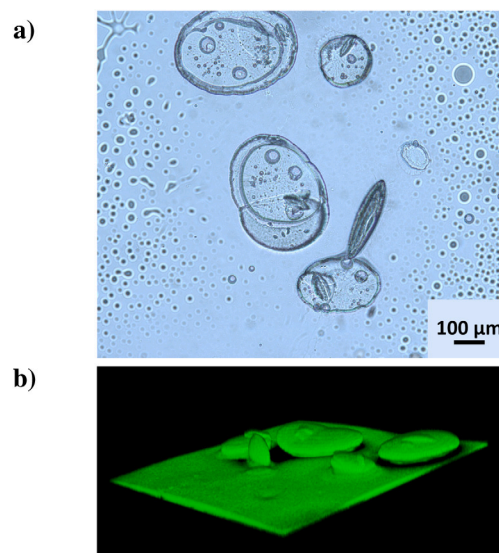


Fig. 5. Light (top) and fluorescence (bottom) microscopy images illustrating the lentil-like morphology and random orientation of HSA crystals grown in presence of $CeCl_3$ (after 9 days). The exact same crystals shown in the top images are depicted in the respective fluorescence microscopy image. a) is a top view on the x - y -plane, while b) is a 3D-representation of z -stacked images (where the z -axis is rescaled by a factor of 1.8 for illustration purposes).

growth curves were found to exhibit a similar monotonically increasing trend with time, we conclude that it is sufficient to compare only the “final” size of the crystals (after 14 days), for comparing crystal sizes and the implied growth kinetics. The crystal sizes after 14 days of the largest crystal for each sample are given in Fig. 2c as a function of c_s . We find that the crystal size (after 14 days) reaches a maximum shortly above c^* , then decreases again. This supports the notion that the most favorable conditions for crystallization, are found close to the phase boundary. Even though the maximum of the nucleation density peak is slightly shifted compared to the maximum of crystal size, we still observe a remarkably similar sharp trend favoring salt concentrations shortly after exceeding c^* for maximum growth.

4. IV. Conclusions

Using HSA with $CeCl_3$ as a model system, this study aimed at connecting protein crystallization kinetics to the phase diagram.

The nucleation density data reveal that for this system, crystals are only found in the lower part of regime II. Intriguingly, the nucleation density peaks shortly above c^* and then decays rapidly, potentially due to the increased occupation of binding sites at the HSA molecules with higher c_s and the associated changes in interaction [18,19,26].

In the analysis of nucleation kinetics, the model of a sigmoidal dependence of the nucleation density on time was successfully applied to the HSA- $CeCl_3$ system, similar to what has been reported for various other systems [35,39,50]. The analysis of the kinetic data showed that the onset (t_c) decreases and the characteristic rate of the nucleation (k) increases with the protein concentration c_p when conditions with constant distances from the phase boundaries are compared. This suggests that a similar mechanism underlies the nucleation process, the speed of which (in terms of k and t_c) is determined by c_p (*i.e.*, diffusion-limited), with variations only at high c_p .

All crystallization conditions studied here lie in the vicinity of the extrapolated bulk LLPS loop. We note that the occurrence of LLPS does not appear to be the sole mechanism for the rapid decrease in nucleation density and rate. Possible effects such as density fluctuations or a decreased activation energy barrier on the one hand and a reduced protein concentration due to dense phase formation on the other hand

appear to work in opposite directions or do not significantly impact the crystallization process under the present conditions.

Similar to the nucleation density and rate, the maximum crystal size was found to peak slightly above c^* . Thus, all parameters studied show a strong, sharp peak in the lower regime II: Based on these results, it is reasonable to conclude that a particular location in the phase diagram, namely shortly after c_s surpasses c^* , is favorable for nucleation and crystal growth.

Furthermore, the comparison with B_2/B_2^{HS} data suggests that the reduced second virial coefficient alone fails to explain the intricacies of the observed trends, as it does not reflect a sharp attractive minimum. This emphasizes the importance of c_s , which goes beyond controlling the interactions, as the salt cations are physically incorporated into the crystal lattice. We speculate that, in addition to direct protein–protein contacts, the observed trends are related to the specific and local interactions induced by ion-activated patches, for which there may be favorable conditions at a specific stoichiometry.

Declaration of competing interest

The authors declare that they have no known competing financial interests or personal relationships that could have appeared to influence the work reported in this paper.

Acknowledgments

We gratefully acknowledge experimental assistance by Ralf Zenke and Jofre Herrera Ossó, financial support of the DFG (SCHR700/39-1) and the hospitality of the ILL (Grenoble) where part of this work was performed.

Appendix A. Supplementary data

Supplementary material related to this article can be found online at <https://doi.org/10.1016/j.jcrysgro.2022.126959>.

References

- [1] J. Holcomb, N. Spellmon, Y. Zhang, M. Doughan, C. Li, Z. Yang, Protein crystallization: Eluding the bottleneck of X-ray crystallography, *AIMS Biophys.* 4 (2017) 557.
- [2] I. Staneva, D. Frenkel, The role of non-specific interactions in a patchy model of protein crystallization, *J. Chem. Phys.* 143 (2015) 194511.
- [3] M. Lund, Anisotropic protein–protein interactions due to ion binding, *Colloids Surfaces B* 137 (2016) 17.
- [4] G.A. Vliegthart, H.N.W. Lekkerkerker, Predicting the gas–liquid critical point from the second virial coefficient, *J. Chem. Phys.* 112 (2000) 5364, <http://dx.doi.org/10.1063/1.481106>.
- [5] F. Zhang, Nonclassical nucleation pathways in protein crystallization, *J. Phys.: Condens. Matter* 29 (2017) 443002.
- [6] P.G. Vekilov, Nucleation of protein condensed phases, *Rev. Chem. Eng.* 27 (2011) 1.
- [7] P.G. Vekilov, The two-step mechanism of nucleation of crystals in solution, *Nanoscale* 2 (2010) 2346.
- [8] D. James, S. Bearsto, C. Hartt, O. Zavalov, I. Saika-Voivod, R.K. Bowles, P.H. Poole, Phase transitions in fluctuations and their role in two-step nucleation, *J. Chem. Phys.* 150 (2019) 074501.
- [9] D.V. Alexandrov, I.G. Nizovtseva, On the theory of crystal growth in metastable systems with biomedical applications: protein and insulin crystallization, *Phil. Trans. R. Soc. A* 377 (2019) 20180214.
- [10] C. Haas, J. Drenth, Understanding protein crystallization on the basis of the phase diagram, *J. Cryst. Growth* 196 (1999) 388.
- [11] S. Whitelam, Control of pathways and yields of protein crystallization through the interplay of nonspecific and specific attractions, *Phys. Rev. Lett.* 105 (2010) 088102.
- [12] S. Karthika, T. Radhakrishnan, P. Kalaichelvi, A review of classical and nonclassical nucleation theories, *Cryst. Growth Des.* 16 (2016) 6663.
- [13] M. Sleutel, A.E. Van Driessche, Nucleation of protein crystals—A nanoscopic perspective, *Nanoscale* 10 (2018) 12256.
- [14] P.G. Vekilov, Dense liquid precursor for the nucleation of ordered solid phases from solution, *Cryst. Growth Des.* 4 (2004) 671.
- [15] K.E. Blow, D. Quigley, G.C. Sosso, The seven deadly sins: When computing crystal nucleation rates, the devil is in the details, *J. Chem. Phys.* 155 (2021) 040901.
- [16] S. Curry, H. Mandelkow, P. Brick, N. Franks, Crystal structure of human serum albumin complexed with fatty acid reveals an asymmetric distribution of binding sites, *Nat. Struct. Biol.* 5 (1998) 827.
- [17] S. Sugio, A. Kashima, S. Mochizuki, M. Noda, K. Kobayashi, Crystal structure of human serum albumin at 2.5 Å resolution, *Protein Eng. Des. Select.* 12 (1999) 439.
- [18] F. Zhang, G. Zocher, A. Sauter, T. Stehle, F. Schreiber, Novel approach to controlled protein crystallization through ligandation of yttrium cations, *J. Appl. Crystallogr.* 44 (2011) 755.
- [19] A. Sauter, M. Oelker, G. Zocher, F. Zhang, T. Stehle, F. Schreiber, Nonclassical pathways of protein crystallization in the presence of multivalent metal ions, *Cryst. Growth Des.* 14 (2014) 6357.
- [20] O. Matsarskaia, F. Roosen-Runge, F. Schreiber, Multivalent ions and biomolecules: Attempting a comprehensive perspective, *ChemPhysChem* 21 (2020) 1742.
- [21] Y. Guo, N. Nishida, T. Hoshino, Quantifying the separation of positive and negative areas in electrostatic potential for predicting feasibility of ammonium sulfate for protein crystallization, *J. Chem. Inform. Model.* 61 (2021) 4571.
- [22] R.P. Hegde, G.C. Pavithra, D. Dey, S.C. Almo, S. Ramakumar, U.A. Ramagopal, Can the propensity of protein crystallization be increased by using systematic screening with metals? *Prot. Sci.* 26 (2017) 1704.
- [23] A. Bijelic, A. Rompel, The use of polyoxometalates in protein crystallography—An attempt to widen a well-known bottleneck, *Coord. Chem. Rev.* 299 (2015) 22.
- [24] F. Roosen-Runge, F. Zhang, F. Schreiber, R. Roth, Ion-activated attractive patches as a mechanism for controlled protein interactions, *Sci. Rep.* 4 (2014) 7016.
- [25] R. Maier, G. Zocher, A. Sauter, S. Da Vela, O. Matsarskaia, R. Schweins, M. Sztucki, F. Zhang, T. Stehle, F. Schreiber, Protein crystallization in the presence of a metastable liquid–liquid phase separation, *Cryst. Growth Des.* 20 (2020) 7951.
- [26] R. Maier, M.R. Fries, C. Buchholz, F. Zhang, F. Schreiber, Human versus bovine serum albumin: A subtle difference in hydrophobicity leads to large differences in bulk and interface behavior, *Cryst. Growth Des.* 21 (2021) 5451.
- [27] H.A. Sober, *Handbook of Biochemistry: Selected Data for Molecular Biology*, second ed., CRC Press, Cleveland, 1970.
- [28] C. Lin, Y. Zhang, J.J. Liu, X.Z. Wang, Study on nucleation kinetics of lysozyme crystallization, *J. Cryst. Growth* 469 (2017) 59.
- [29] V. Bhamidi, E. Skrzypczak-Jankun, C. Schall, Dependence of nucleation kinetics and crystal morphology of a model protein system on ionic strength, *J. Cryst. Growth* 232 (2001) 77, [http://dx.doi.org/10.1016/S0022-0248\(01\)01143-5](http://dx.doi.org/10.1016/S0022-0248(01)01143-5).
- [30] M. Amiri, K. Jankeje, J.R. Albani, Origin of fluorescence lifetimes in human serum albumin. Studies on native and denatured protein, *J. Fluorescence* 20 (2010) 651.
- [31] J. Schindelin, I. Arganda-Carreras, E. Frise, V. Kaynig, M. Longair, T. Pietzsch, A. Cardona, Fiji: an open-source platform for biological-image analysis, *Nature Methods* 9 (2012) 676.
- [32] B. Schmid, J. Schindelin, A. Cardona, A high-level 3D visualization API for Java and ImageJ, *BMC Bioinformatics* 11 (2010) 274.
- [33] J.D. Schmit, K. Dill, Growth rates of protein crystals, *J. Am. Chem. Soc.* 134 (2012) 3934.
- [34] A. George, W.W. Wilson, Predicting protein crystallization from a dilute solution property, *Acta Crystall. Sect. D* 50 (1994) 361.
- [35] C.N. Nanev, V.D. Tonchev, Sigmoid kinetics of protein crystal nucleation, *J. Cryst. Growth* 427 (2015) 48.
- [36] D. Soraruf, F. Roosen-Runge, M. Grimaldo, F. Zanini, R. Schweins, T. Seydel, F. Zhang, R. Roth, M. Oettel, F. Schreiber, Protein cluster formation in aqueous solution in the presence of multivalent metal ions – a light scattering study, *Soft Matter* 10 (2014) 894.
- [37] P.R.t. Wolde, D. Frenkel, Enhancement of protein crystal nucleation by critical density fluctuations, *Science* 277 (1997) 1975.
- [38] M. Wolf, F. Roosen-Runge, F. Zhang, R. Roth, M.W. Skoda, R.M. Jacobs, M. Sztucki, F. Schreiber, Effective interactions in protein–salt solutions approaching liquid–liquid phase separation, *J. Mol. Liq.* 200 (2014) 20.
- [39] D.A. Barlow, J. Gregus, The kinetics of homogeneous and two-step nucleation during protein crystal growth from solution, *Int. J. Chem. Kinet.* 51 (2019) 840.
- [40] O. Galkin, P.G. Vekilov, Direct determination of the nucleation rates of protein crystals, *J. Phys. Chem. B* 103 (1999) 10965, <http://dx.doi.org/10.1021/jp992786x>.
- [41] O. Galkin, P.G. Vekilov, Are nucleation kinetics of protein crystals similar to those of liquid droplets? *J. Am. Chem. Soc.* 122 (2000) 156, <http://dx.doi.org/10.1021/ja9930869>.
- [42] D.N. Petsev, K. Chen, O. Gliko, P.G. Vekilov, Diffusion-limited kinetics of the solution–solid phase transition of molecular substances, *Proc. Natl. Acad. Sci.* 100 (2003) 792.
- [43] M. Pusey, R. Naumann, Growth kinetics of tetragonal lysozyme crystals, *J. Cryst. Growth* 76 (1986) 593.
- [44] M. Muschol, F. Rosenberger, Liquid–liquid phase separation in supersaturated lysozyme solutions and associated precipitate formation/crystallization, *J. Chem. Phys.* 107 (1997) 1953.

- [45] Y.G. Kuznetsov, A.J. Malkin, A. McPherson, The liquid protein phase in crystallization: a case study—intact immunoglobulins, *J. Cryst. Growth* 232 (2001) 30.
- [46] A.A. Chernov, Protein crystals and their growth, *J. Struct. Biol.* 142 (2003) 3.
- [47] P.E. L'vov, A.R. Umantsev, Two-step mechanism of macromolecular nucleation and crystallization: Field theory and simulations, *Cryst. Growth Des.* 21 (2020) 366.
- [48] R. Maier, B. Sohmen, S. Da Vela, O. Matsarskaia, C. Beck, R. Schweins, T. Seydel, F. Zhang, F. Schreiber, Protein crystallization from a preordered metastable intermediate phase followed by real-time small-angle neutron scattering, *Cryst. Growth Des.* 21 (2021) 6971.
- [49] J.F. Lutsko, How crystals form: A theory of nucleation pathways, *Sci. Adv.* 5 (2019) eaav7399.
- [50] A. Sauter, F. Roosen-Runge, F. Zhang, G. Lotze, R.M.J. Jacobs, F. Schreiber, Real-time observation of nonclassical protein crystallization kinetics, *J. Am. Chem. Soc.* 137 (2015) 1485.
- [51] F. Zhang, R. Roth, M. Wolf, F. Roosen-Runge, M.W.A. Skoda, R.M.J. Jacobs, M. Sztucki, F. Schreiber, Charge-controlled metastable liquid–liquid phase separation in protein solutions as a universal pathway towards crystallization, *Soft Matter* 8 (2012) 1313.